

Height-dependent meteor temperatures and comparisons with lidar and OH measurements¹

W.K. Hocking, P.S. Argall, R.P. Lowe, R.J. Sica, and H. Ellinor

Abstract: A new method is introduced that allows meteor radars to potentially produce height-dependent temperatures, rather than simply averages over the meteor region. The method is applied to data from the Clovar radar, near London, Ontario, and then a three-way comparison between Rayleigh lidar temperatures, hydroxyl temperatures, and meteor temperatures is undertaken. The three methods prove to be complementary. The OH measurements have good accuracy, but suffer slightly from lack of precise knowledge about their height and the fact that they are effectively integrated over the depth of the OH layer. The lidar temperatures are measured at well-defined altitudes and have better accuracy than the meteor method. The meteor temperatures have the largest errors, but still provide sufficient accuracy for many types of atmospheric studies, and have the advantage that these measurements can be made 24 h a day and in all sky conditions (including during cloud and strong sunlight and moonlight). The measurements from these instruments are complementary in that they are useful for studying the temperature on different time and altitude scales.

PACS No.: 94.10.Dy

Résumé : Nous présentons une nouvelle méthode qui potentiellement permet d'utiliser des radars à météore pour déterminer la variation de la température avec l'altitude, plutôt que d'avoir à se contenter d'une valeur moyenne dans la région des météores. Nous appliquons cette technique aux données du radar Clovar près de London en Ontario, et continuons avec une comparaison triple avec les températures lidar Rayleigh et les températures hydroxyles. Les trois méthodes s'avèrent complémentaires. Les mesures OH sont de haute précision, mais souffrent d'incertitude sur l'altitude et du fait qu'elles sont effectivement intégrées sur toute l'épaisseur de la couche OH. Les mesures lidar sont faites à des altitudes bien définies et sont plus précises que celle du radar. La méthode par radar a les marges d'erreur les plus importantes, mais une précision suffisante pour nombres d'études atmosphériques, avec l'avantage de pouvoir être utilisée 24 heures par jour, dans toutes les conditions (beau temps, mauvais temps, à la lumière du soleil ou de la lune). Les mesures de ces différents instruments sont complémentaires en ce qu'ensemble elles sont utiles pour étudier la variation de la température en temps et en altitude.

[Traduit par la Rédaction]

Received 27 January 2006. Accepted 14 October 2006. Published on the NRC Research Press Web site at <http://cjp.nrc.ca/> on 11 April 2007.

W.K. Hocking, P.S. Argall,² R.P. Lowe, R.J. Sica, and H. Ellinor. Department of Physics and Astronomy, Faculty of Science, University of Western Ontario, 1151 Richmond Street, London, ON N6A 3K7, Canada.

¹This paper is published as part of the proceedings of the 32nd Annual European Meeting on Atmospheric Studies by Optical Methods (ASOM) that was held 29 August to 1 September 2005 at the University of Western Ontario, London, Ont.

²Corresponding author (e-mail: pargall@uwo.ca).

1. Introduction

Several ground-based techniques exist for the measurement of middle atmosphere temperatures in the altitude range 80 to 95 km altitude, including meteor radar, lidar, and hydroxyl rotational methods. Depending on instrumentation, these techniques produce averages over different volumes of the atmosphere and for different times of day, each technique having advantages and disadvantages. Comparisons of these methods allow for better use and understanding of the respective measurements. In this paper, we first further develop the basic theory used for temperature determinations by meteor methods, permitting height-dependent temperatures to be found. We then carry out a detailed three-instrument comparison of temperatures measured above London, Ontario (43°N, 81°W), for the period from 1996 to 2001.

Comparisons of previously developed meteor radar temperature techniques with other instruments have been made [1, 2]. She and Lowe [3] showed, using monthly means, that the OH temperature was a good proxy for the 87 ± 4 km temperature.

2. Measurement techniques

2.1. Meteor radar temperatures

The meteor temperatures were determined from measurements made with the Clovar all-sky meteor radar located near the University of Western Ontario in Canada. The system has been described by Hocking and Thayaparan (1997) [4], and was an early version of the SKiYMET radar described by Hocking et al. [5]. The radar employs a 10 kW peak-power transmitter operating at 40.68 MHz, which transmits 13.33 μ s pulses through a single, vertically directed, four-element Yagi antenna. The back-scattered signal is received on five separated two-element Yagis. These receiving antennas are in the form of an asymmetric cross, with two perpendicular arms having lengths of 2.0 wavelengths, and the other pair of perpendicular arms having lengths of 2.5 wavelengths. Whenever a meteor trail with suitable alignment is produced in the sky the transmitted pulses of radiation are partially reflected back to the receiver antennas. Each receiving antenna is connected via equal phase-length cables to separate inputs, and the signals from these inputs are multiplexed on a pulse-to-pulse basis through a single receiver. The in-phase and quadrature components from the receiver are then digitized, allowing interferometry to be used to determine the location of the meteor in the sky (see, for example, refs. 6 and 5). Once the meteors have been positively identified, characteristics such as radial drift speed, decay time, amplitude, and the speed at which the meteor entered the atmosphere are determined. These parameters allow calculation of the temperature, upper atmosphere wind speeds, and ambipolar diffusion coefficients.

2.2. Lidar temperatures

The Purple Crow lidar (PCL) is located at The University of Western Ontario's Delaware Observatory (42°52'N, 81°23'W), approximately 26 km south-south-west of the Clovar radar. The PCL uses two transmitter beams to allow simultaneous Rayleigh, Raman, and sodium-resonance fluorescence measurements. Only temperatures derived from the Rayleigh channel are used in this investigation since there are insufficient sodium temperature measurements currently available to permit them to also be included in the study. The Rayleigh-scatter transmitter uses an Nd:YAG laser that generates 600 mJ/pulses at the second harmonic frequency, 532 nm, at a 20 Hz pulse repetition rate. The PCL receiver uses a 2.65 m diameter liquid mercury mirror as the receiver. The mercury is spun at 10 rpm in a container to produce a reflective, paraboloidal surface. For Rayleigh lidar measurements the intensity of the backscattered light is recorded as a function of altitude at the transmitted wavelength. The details of the temperature processing algorithms are given by [7] and references therein.

2.3. Hydroxyl rotational temperatures

The hydroxyl rotational temperatures were derived from spectra of the hydroxyl airglow obtained using a Fourier transform spectrometer, the UWOMI Michelson Interferometer (UWOMI-3) [3]. The UWOMI, co-located with the PCL, used a liquid nitrogen-cooled germanium detector to measure an interferogram of the zenith sky in the spectral region 1000–1650 nm approximately every 30 s. The temperatures used in this study are the nightly means of the individual 30 s temperature measurements. Temperatures derived from the hydroxyl (3–1) band were used exclusively in the analysis as this band has a high signal-to-noise ratio [8]. Some lines of the (3–1) band are subject to absorption by telluric water vapour. This potential source of error is avoided by using only the three strongest lines of the P1 branch in the temperature analysis, since these lines do not show significant absorption [9].

3. Height-dependent meteor temperatures

Chilson et al. [10], and Hocking et al. [11] proposed using the expression

$$D = K_a T^2 / P \quad (1)$$

combined with pressures P from the COSPAR (Committee on Space research) international reference atmosphere (CIRA) [12], and theoretical estimates of the constant K_a , to determine temperatures at mesopause heights from measurements of the ambipolar coefficient D deduced from meteor decay times. This technique is subsequently referred to as the “Pressure-based” (PB) method. If P and K_a can be accurately determined, then the PB method would be able to provide temperature measurements with useful accuracy. However, it has been shown that uncertainties in both the CIRA pressures and in the constant K_a lead to generally unacceptable uncertainties in temperatures with this method. A second method for determination of temperatures from meteor radar that does not require explicit knowledge of either K_a or P has been proposed [13] and subsequently improved upon [1]. This method requires knowledge of the temperature gradient, which is taken from the study by Hocking et al. [1]; it will be referred to as the “temperature gradient” (TG) method. The TG method is restricted to the determination of weighted mean temperatures in the region between 80 and 95 km, where the weighting is determined by the meteor trail height distribution. Temperature gradients used for the TG method were determined using a global climatology of rocket and lidar data [1].

In this article, we examine the possibility of using the TG method (mean temperature) to determine an approximation for the term K_a/P at the height of measured meteor maximum, and then applying this in the application of the PB method to determine height-dependent temperatures. This combination of the TG and PB methods is referred to as the “temperature gradient + extrapolation” (TGE) method. We are particularly interested in the likely errors implicit in this temperature determination method.

To employ the TGE method, we first consider the expression (1) at two distinct height, designated $z = z_0$, (the height of maximum meteor count rate) and $z = z_h$, where z_h is a nearby height, generally within ± 5 km of z_0 . Then if we apply (1) at each height, and divide the two expressions, and rearrange, the following equation is obtained:

$$\frac{T_z}{T_0} = \sqrt{\frac{D_z \cdot P_z}{D_0 \cdot P_0}} \quad (2)$$

The constant K_a has disappeared. We may now use the hydrostatic equation in the form

$$P_z = P_0 \exp\left(-\int_{z_0}^{z_h} \frac{1}{H} dz\right) \quad (3)$$

where $H = RT/Mg$, R is the ideal gas constant, $T = T(z)$ is the height-dependent temperature, M is the mean molecular mass (28.8 g), and g is the acceleration due to gravity. Explicit calculation of

this integral is not possible since the height-dependent temperature is not known. We, therefore, need to approximate the expression. One possibility is to simply replace the height-dependent term H by a constant value H_0 , where H_0 is determined from the mean height specified by the TG method discussed above. An alternative is to assume that H_0 applies at the height of maximum count rate, and a new scale height H_z applies at the height of interest z_h . Then we can replace $1/H$ in (3) by the mean inverse scale height, viz H_* , where

$$\frac{1}{H_*} = \frac{1}{2} \left(\frac{1}{H_0} + \frac{1}{H_z} \right)$$

Thus, we have two possible expressions, namely,

$$P_z = P_0 \exp \left(-\frac{(z_h - z_0)}{H_0} \right) \quad (4)$$

and

$$P_z = P_0 \exp \left(-\frac{(z_h - z_0)}{H_*} \right) \quad (5)$$

Neither is exact, since H is neither the actual scale height at z_0 , nor the mean value between z_h and z_0 . However, our intent is to compare the two expressions. If they lead to very different answers, then it will be considered inappropriate to employ either procedure. If the differences show small errors, then it will be considered that the method has some viability, irrespective of which value of the scale height is chosen.

First, expressions (4) and (5) are substituted into (2), giving

$$\frac{T_z}{T_0} = \left(\frac{D_z}{D_0} \right)^{1/2} \exp \left(\frac{-(z_h - z_0)}{2H'} \right) \quad (6)$$

where H' is either H_0 or H_* , depending on whether (4) or (5) is employed. In the first case, calculation of T_z is simple, whereas in the second case T_z appears on both the left- and right-hand sides of the equation (in the case of the right-hand side, H_* depends on T_z), but T_z can still be found using numerical procedures. The diffusion coefficients D_z and D_0 are assumed known from experimental measurements of meteor trail decay times.

The estimates of T_z by each procedure will be denoted by T_{z0} and T_{z*} , where the first is determined using the mean scale height H_0 , and the second is determined using the average H_* .

To simplify the following error analysis, it will be assumed that the true temperature at height z_h is given by T_{zt} , with a corresponding scale height H_t .

Dividing the two cases of (6), $H' = H_0$ and $H' = H_*$, gives

$$\frac{T_{z*}}{T_{z0}} = \exp \left\{ -\frac{1}{2} (z_h - z_0) \left[\frac{1}{2} \left(\frac{1}{H_0} + \frac{1}{H_t} \right) - \frac{1}{H_0} \right] \right\} \quad (7)$$

or

$$\frac{T_{z*}}{T_{z0}} = \exp \left[-\frac{1}{4} (z_h - z_0) \left(\frac{1}{H_t} - \frac{1}{H_0} \right) \right] \quad (8)$$

Applying a Taylor expansion and retaining only first-order terms (since only small displacement $(z_h - z_0)$ — less than a few kilometres — are considered), gives

$$\frac{T_{z*}}{T_{z0}} = 1 - \frac{1}{4} (z_h - z_0) \left(\frac{1}{H_t} - \frac{1}{H_0} \right) \quad (9)$$

or

$$\frac{T_{z0} - T_{z^*}}{T_{z0}} = \frac{1}{4} (z_h - z_0) \left(\frac{1}{H_t} - \frac{1}{H_0} \right) \quad (10)$$

Hence, the relative difference between the two methods is of the order of

$$\frac{\Delta T}{T} = \frac{1}{4} (z_h - z_0) \left(\frac{Mg}{R} \right) \left(\frac{1}{T_{zt}} - \frac{1}{T_0} \right) \quad (11)$$

or

$$\frac{\Delta T}{T} = 8.2 (z_h - z_0) \left(\frac{1}{T_{zt}} - \frac{1}{T_0} \right) \quad (12)$$

where the heights are in kilometres and the temperatures are in Kelvin, and where we have taken M to be 28.8 g/mol, and $g = 9.5 \text{ m s}^{-2}$ at 90 km altitude.

Taking a representative case of a temperature change of 20 K for a height change of 5 km, at a typical midlatitude temperature of $T_0 = 200 \text{ K}$ (and assuming $T_{zt} = 220 \text{ K}$), gives a relative error with a magnitude of about 1.9%, or approximately 4 K. For a height change of 3 km, the same temperature differential would give a 1.1% error, or about 2 K. Smaller temperature differentials would give smaller errors. During the polar summer at mesopause heights, the mean temperature can be as low as 120 K, so using $T_{zt} = 120 \text{ K}$, $T_0 = 140 \text{ K}$, and a height difference of 5 km, gives an error of about 5%, or 6 K. These errors are less than the errors in T_0 discussed in ref. 1, although the new errors have the additional risk that they may be systematic rather than random. They also tend to be greatest when the mean temperatures are smallest, and so are likely to be least accurate in the polar summer, when temperatures are coldest.

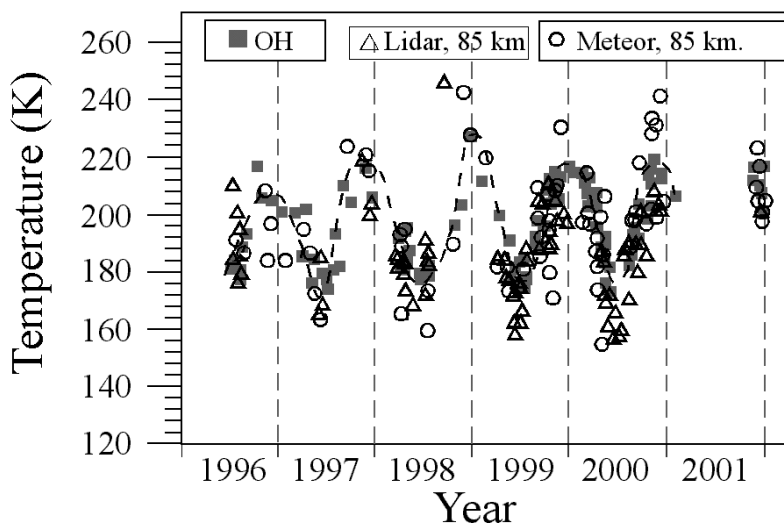
It is therefore proposed that (6) may be applied with either version of H' , provided that it is recognized that additional errors of up to 5–6 K may result for a height displacement of 3–5 km. We will generally use $H' = H_0$ in our calculations.

3.1. Data sets — similarities and differences

Two different meteor temperature determination methods are used in the following comparisons. The first is the “single-height”, TG, temperature, which is a weighted average across the meteor region. It will be referred to as T_{pk} , where the “pk” refers to “peak”. The second is the TGE height-dependent method developed in the previous section. Temperatures derived using the TGE method are given at 3 km intervals (85, 88, 91, and 94 km) and are averaged over 3 km. These data are compared with the lidar data, which are averaged over the same altitude intervals. The meteor temperatures used in this study are the average of 48 h of measurements. This data length is required as the method relies on the assumed seasonal temperature gradient, and for accurate temperatures, this model should be approximately valid for the measurement interval. For periods of a day or less tidal variations in the temperature gradient can bias the derived temperatures. For short periods, for example, tidal studies, an alternative approach has been developed [14]. The 2 d interval used for the radar measurements was chosen to overlap optical measurements (either the lidar or OH, whichever was relevant).

The meteor radar ran continuously throughout the times compared, except for short downtimes due to power failures and system repairs. The lidar and hydroxyl rotational data were obtained when observing conditions were favourable with the sky being dark and relatively cloud free. There are 111 dates when meteor radar and lidar temperatures were of sufficient quality for comparisons, and 132 dates available for meteor and hydroxyl temperature comparisons. However, on some occasions the meteor data quality was insufficient to permit a height-dependent determination, or possibly could not produce a useful measurement at the lowest available height, and on occasion the lidar data were

Fig. 1. Time-series of OH, meteor (85 km), and lidar (85 km) temperatures during the years 1996–2001. The annual cycle is highlighted by a hand-drawn broken line. Only dates for which at least two of the instruments made common observations are shown — the full data sets for each individual instrument are much larger. Data for 2002 are not shown, but show similar general characteristics.



unable to produce measurements at some heights. Hence, the number of days of overlap listed for the comparisons discussed below is usually less than the total number of days of overlap, and can vary with height.

The hydroxyl rotational temperatures represented a weighted average over an emission layer that typically extends over more than one scale height. The shape of this emission layer is sensitive to changes in the number density of O and H. Though passive optical instruments can rapidly achieve extremely high signal-to-noise ratio measurements of the bright emission (and thus temperature fluctuations), the interpretation of these fluctuations involves a convolution of the actual temperature change and the changes in the height of the OH emission layer. Dynamics further complicate the interpretation of the temperatures, as atmospheric waves can transport O and H vertically and horizontally.

In considering these comparisons, the differences in the fields of view of the instruments should be remembered. The PCL's field of view is 0.39 mrad, the hydroxyl spectrometer views a field about 5° across, and the meteor radar's field of view is much larger again, out to $\pm 60^\circ$ from zenith. However, it needs to also be recognized that once nightly averaging of the temperatures is performed, significant spatial and temporal averaging is also implicit with all three techniques, as the atmosphere moves through the instruments' fields of view.

Two lidar data sets are used in this comparison, which will be denoted "raw" and "tidal". Raw data are the average temperatures for the observation period, which typically range from 2 to 8 h in length and usually start within 1 h of sunset. The tidal data have had a correction for the diurnal and semi-diurnal, migrating and nonmigrating, tides applied. The tidal correction is applied to make the data set more consistent with the diurnally averaged meteor data. The tidal correction applied to the lidar temperatures is derived from GSWM-02 [15]. The OH measurements show a similar temporal bias to those of the lidar. The meteor measurements suffer from far less temporal bias, but nevertheless a bias does still exist in that the meteors detection rate peaks at around 3–6 a.m. local time, see, for example, Hocking et al. [16].

3.2. Comparison methods

The main objective of this study is to determine whether the lidar, hydroxyl rotational, and meteor radar temperature two daily averages are consistent with each other and to examine reasons for any differences. The methods of comparison involve studies of mean temperatures and the variability on a measurement-by-measurement basis.

Figure 1 shows the temperature variations as a function of time for the period 1996 to 2001. The optical data sets overlap for the period 1994 to 2002, with lidar data existing from 1994 onward, and OH data from 1991 to 2001. Radar data are available starting from 1996. Only temperatures where measurements from two or more instruments overlapped is shown in Fig. 1 — much better data density is available if all the data from just one method (especially the meteor data) is used. As expected, an annual cycle, with colder summer temperatures, is seen in each of the data sets. The broken line in Fig. 1 is meant as a guide to show the seasonal variation in temperature. The OH temperatures appear to have smaller variations than the lidar and meteor temperatures.

Table 1 shows a summary of all of the comparisons carried out. The parameters in Table 1 are described in the table caption. Specifics about the methods of determination of the parameters shown in Table 1 will now be described in more detail.

It should be noted in advance that means from one data set to the next, for a particular instrument, may show some small variations. For example, the second row in Table 1 (Meteor, peak) lists the mean temperatures for the comparisons with the lidar at 85, 88, and 91 km as 192.0, 192.3, and 191.7 K, respectively. These temperature differences are due to the different data sets used for each comparison. The lidar data sets are different for each altitude, since the number of lidar measurements available decreases as altitude increases. Because the radar data set is matched to the lidar data set, the radar data set also changes and, therefore, the mean changes slightly.

The inter-comparison between the three data sets is done using a regression analysis that makes no assumptions about the errors in either data set; rather it lets the errors be free variables [16, 17]. A line fit is performed by finding the regression of the ordinate on the abscissa, (which effectively assumes zero error in the abscissa), and then a regression of the abscissa on the ordinate (which effectively assumes zero error in the ordinate) is determined. An example of this is shown in Fig. 2a, with the two continuous lines showing the two corresponding best fit lines. However, the actual best fit line could be anywhere between these two extremes, and depends on the errors associated with the individual measurements.

Figure 2b shows the slope and errors in the two data sets. These errors were deduced by the method of Hocking et al. [16]. The lower abscissa and the ordinate are both plotted linearly, and then the curve of g_0 values is applied. The upper axis is not determined until after the g_0 curve has been produced, and the axis is then scaled according to the expected relation between g_0 and σ_x , which explains why it is nonlinear. The specific spacing of values on the upper axis therefore changes from graph to graph. (An alternative presentation that plots the data using two curves on two linear axes is given in ref. 17). Two sets of lines are shown on Fig. 2b — the first is a vertical line at $\sigma_{OH} = \sigma_{Met} = 8.1$ K, and represents the case that the two variances are equal. The horizontal arrow that points to the left from this line shows the value of g_0 that occurs if the errors for the two methods are assumed to be equal. The second set of broken lines comprises a horizontal line at $g_0 = 1$ and a corresponding vertical line that shows the values of the two errors when $g_0 = 1$ is assumed. This case corresponds to the (unattainable) ideal case where the two instruments measure exactly the same quantity, in this case the temperature at the same time and the same location and with the same field of view. In this case the corresponding errors are $\sigma_{OH} = 4$ K and $\sigma_{Met} = 11.6$ K.

In Table 1, we present the errors determined using this method. However, it needs to be noted that a slope of 1 may not always be optimum as the different measurement techniques have different spatial and temporal resolution. For example, if the OH layer thickness were greater than the averaging used for the lidar temperatures this may reduce the variations in the OH temperatures compared to the lidar temperatures, changing the value of g_0 . If g_0 is reduced then σ_x decreases and σ_y increases. There are

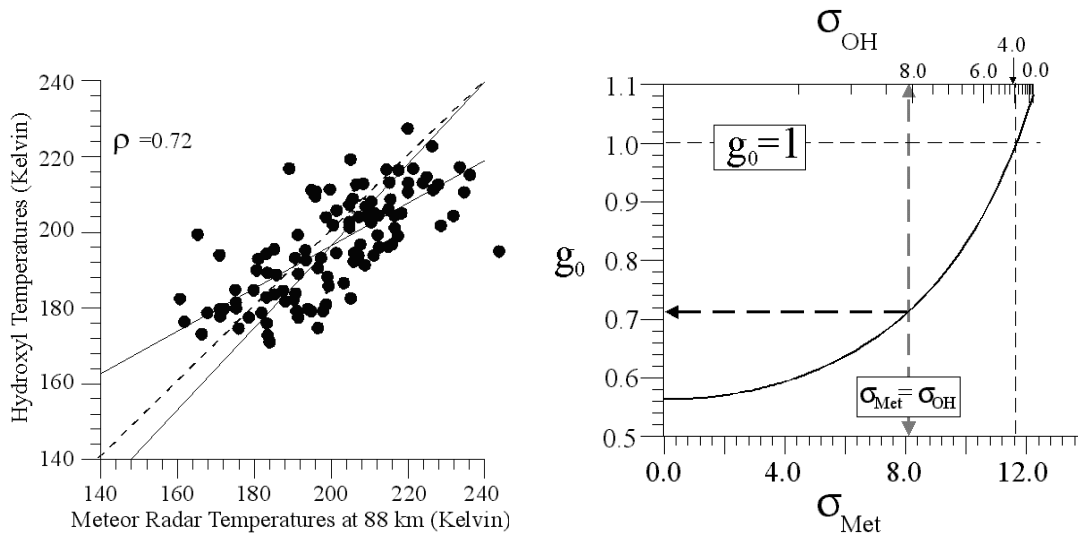
Table 1. Relationships between mean values, correlation coefficients, and error estimates for comparisons between the different instruments. The first line in each box gives the mean temperature and standard error for the data-set described in the same row and in the left-hand column, and the second set of values is the mean and standard error for the data-set described in the same column and in the top row. The third quantity is the zero-lag correlation coefficient. The next pair of numbers are the errors that would be associated with individual measurements of each data point if it can be assumed that the slope of the best-fit line were unity. The last number is the number of points in each data-comparison. Note that because each comparison involves a different subset of data, the means cannot be compared between data sets. For example, the points used for comparing the meteor data at 85 km and the lidar data at 85 km would be a different data-set to that used to compare say the OH temperatures and the 85 km lidar data.

Lidar, 85 km, raw	Lidar, 88 km, raw	Lidar, 91 km, raw	Lidar, 85 km, tidal	Lidar, 88 km, tidal	Lidar, 91 km, tidal	OH
Meteor, peak, 24 h						
192.0, 1.6	192.3, 1.7	191.7, 1.9	192.0, 1.6	192.3, 1.7	191.7, 1.9	198.2, 1.5
180.1, 1.5	179.5, 1.5	184.2, 1.6	184.8, 1.5	183.3, 1.4	184.5, 1.6	196.6, 1.3
$\rho = 0.653$	$\rho = 0.705$	$\rho = 0.506$	$\rho = 0.651$	$\rho = 0.695$	$\rho = 0.476$	$\rho = 0.637$
10, 9	10.5, 6	13, 8	10, 8	11, 5	13.5, 8	11, 7
104	97	85	104	97	85	114
Meteor, 85 km, 24 h						
183.1, 2.6			183.1, 2.6			196.5, 2.3
182.6, 1.7			187.3, 1.7			199.9, 1.3
$\rho = 0.621$			$\rho = 0.626$			$\rho = 0.706$
18, 4			18, 2			16, 0
81			81			95
Meteor, 88 km, 24 h						
	192.6, 2.0			192.6, 1.9		200.0, 1.6
	179.4, 1.5			183.3, 1.9		196.6, 1.3
	$\rho = 0.713$			$\rho = 0.703$		$\rho = 0.720$
	13, 4			13, 3		12, 0
	97			97		116
Meteor, 91 km, 24 h						
		189.5, 1.8			189.5, 1.5	195.6, 1.4
		184.2, 1.6			184.5, 1.8	196.5, 1.3
		$\rho = 0.541$			$\rho = 0.515$	$\rho = 0.659$
		12, 8			12, 8	10, 1
		84			84	116
Meteor, 85 km, night						
181.7, 2.6			181.7, 2.6			197.3, 2.2
182.4, 1.8			187.2, 1.8			201.4, 1.3
$\rho = 0.596$			$\rho = 0.595$			$\rho = 0.678$
14, 0			16, 5			14, 0
65			65			81
Meteor, 88 km, night						
	190.8, 2.1			190.8, 2.1		198.1, 1.9
	179.8, 1.6			183.6, 1.5		196.8, 1.3
	$\rho = 0.616$			$\rho = 0.592$		$\rho = 0.666$
	15, 6			15, 5		15, 0
	89			89		108

Table 1. (concluded).

	Lidar, 85 km, raw	Lidar, 88 km, raw	Lidar, 91 km, raw	Lidar, 85 km, tidal	Lidar, 88 km, tidal	Lidar, 91 km, tidal	OH
Meteor, 91 km, night							
			190.3, 1.9			190.3, 1.9	
			185.0, 1.6			185.0, 1.6	
			$\rho = 0.472$			$\rho = 0.472$	
			14, 9			14, 9	
			78			78	
OH	190.8, 1.5	191.3, 1.6	190.5, 1.6	190.8, 1.5	191.2, 1.6	190.5, 1.8	
	183.3, 1.8	185.5, 1.9	188.2, 1.8	188.0, 1.8	189.0, 1.8	188.5, 2.2	
	$\rho = 0.770$	$\rho = 0.730$	$\rho = 0.526$	$\rho = 0.762$	$\rho = 0.710$	$\rho = 0.502$	
	3, 10	5.5, 11	8, 14	4, 11	6, 9	9, 12	
	90	80	64	90	80	64	

Fig. 2. (a) Scatter plot of 2 d average temperatures deduced by OH measurements (night time only) and meteor methods at 88 km. In this case, the meteor temperatures were deduced using data from both daytime and night-time (i.e., using a full 48 h of data). The broken line shows a 1:1 ratio, and the two continuous lines show least-squares fits for the regression of the abscissa on the ordinate, and the regression of the ordinate on the abscissa. (b) The graph shows the possible acceptable combinations of g_0 , σ_{Met} , and σ_{OH} , where g_0 is the slope, σ_{Met} , and σ_{OH} are the corresponding errors for the abscissa and ordinate. The extrema correspond to the cases shown for the two best-fit lines in Fig. 2a, i.e., regression of OH on Met, and conversely, and so correspond to cases where the error in Met is first assumed to be zero, and then the error in OH is assumed to be zero. The true situation lies between these extrema, and the curve shows possible combinations. For example, if it is assumed that $\sigma_{Met} = \sigma_{OH}$, then the optimum slope is 0.73 and $\sigma_{Met} = \sigma_{OH} = 8.2$. If it is assume that the optimum slope should be unity, then it requires that $\sigma_{Met} = 11.6$ and $\sigma_{OH} = 4.0$ K.



places in a Table 1 where $\sigma_{OH} = 0$, which is unrealistic and likely indicating that the appropriate slope is less than unity.

Typical errors from Table 1 indicate that the UWOMI-3 errors are of the order of 4–5 K, lidar

Table 2. Error estimates for the PCL temperatures as a function of altitude.

Altitude (km)	Rayleigh lidar seeding error (K)	Photon noise error (K)	Total error
85	1.6	0.7	1.8
88	2.2	1.2	2.5
91	3.1	2.8	4.2

7–8 K, and meteor 10–14 K. It is important to note that these are not the errors associated solely with the measurement technique but include additional errors due to geophysical variations in temperature over the temporal and spatial scales associated with each technique. Table 2 summarizes the errors associated with the lidar temperatures used in this study, showing that the inherent errors in the lidar temperature measurements vary from 1.8 to 4.2 K. Inherent UWOMI-3 temperature errors are estimated to be approximately 4 K. The meteor error estimates are consistent with other estimates for the meteor peak temperature (TG method) having errors of approximately 8 to 10 K [1], plus an additional error of 5 to 8 K due to the extrapolation process of the TGE method, giving overall expected instrumental errors in the range 10 to 13 K.

3.3. Results

The time series of the data are shown in Fig. 1, and a scatter plot of the OH temperatures and the corresponding 88 km meteor temperatures from the overlapping time periods is shown in Fig. 2a. The continuous lines represent the two best fit lines determined using the procedure described in Sect. 4. The broken line, shown for reference, indicates equal abscissa and ordinate temperatures. The data points on Fig. 2a show a general trend to be spread out along the direction of the lines, which represents real geophysical temperature variability, but there is also significant spread perpendicular to this direction, indicating the degree of variation between the individual OH and meteor radar temperature measurements. The distribution of the data points is such that the average is slightly to the right of the equal temperature (broken) line in this case, indicating that the average of the meteor temperatures is slightly greater than the average of the OH temperatures. However, the differences are not significant at the 95% confidence level when a t-test is employed. Figure 2b shows the relationship between the slope of the fitted line and the errors in the OH temperatures (top axis) and the errors in the meteor temperatures (bottom axis). Assuming that the slope of the best fit line should be unity, ($g_0 = 1$) gives the OH and meteor errors as 4 and 11.6 K, respectively.

To better interpret the results in Table 1, it is important to know about the correlations as a function of height. For example, if the 85 and 88 km data were highly correlated, then a good correlation between the lidar data and the meteor data at 85 km altitude might be simply a side-effect of the good correlation at 88 km, coupled with a natural tendency for the 85 km data to follow the 88 km data. Therefore, we have examined the correlations between different heights using the same instruments, and these can be used as a baseline for considerations about Table 1. The key common-instrument correlations examined are listed below. Errors given are errors for the mean at the one-sigma level.

1. Meteor data at 88 km for whole days coverage compared to meteor data at 88 km for night only: Means = 193.4 ± 1.8 , 191.0 ± 1.9 . $\rho = 0.710$. Assuming $g_0 = 1$ gives $\sigma_{\text{day}} = 9$ and $\sigma_{\text{night}} = 11$. Number of points = 101. If it is assumed that $\sigma_{\text{day}} = \sigma_{\text{night}}$, then $g_0 = 1.07$, $\sigma_{\text{day}} = \sigma_{\text{night}} = 10.2$. This high correlation coefficient is expected since normally day to night variations are governed by the tides, which have amplitudes of typically only a few Kelvin, so that over the time scales considered, seasonal variability dominates the correlation.
2. Meteor data at 91 km for whole day coverage compared to meteor data at 91 km at night only: Means = 191.1 ± 1.6 , 190.1 ± 1.7 . $\rho = 0.676$. Assuming $g_0 = 1$ gives $\sigma_{\text{day}} = 8$, $\sigma_{\text{night}} = 10.5$.

- Number of points = 99. If it is assumed that $\sigma_{\text{day}} = \sigma_{\text{night}}$, then $g_0 = 1.15$, $\sigma_{\text{day}} = \sigma_{\text{night}} = 9.2$.
3. Meteor data at peak height for whole day coverage compared to meteor data at 91 km for whole day:
Means = 192.6 ± 1.6 , 189.9 ± 1.5 . $\rho = 0.998$. Assuming $g_0 = 1$ gives $\sigma_{\text{pk}} = 1.8$, $\sigma_{91} = 1.8$. Number of points = 110. This high correlation is expected since the height of peak meteor counts is generally close to 91 km.
 4. Meteor data at peak height for whole day coverage compared with meteor data at 88 km for whole day:
Means = 192.2 ± 1.6 , 192.6 ± 1.5 . $\rho = 0.958$. g_0 is greater than 1.06. Number of points = 111.
 5. Meteor data at 85 km for whole day coverage compared to meteor data at 91 km for whole day:
Means = 183.3 ± 1.5 , 193.7 ± 1.5 . $\rho = 0.872$. Assuming $g_0 = 1$ gives $\sigma_{85} = 12$, $\sigma_{91} = 0$. Number of points = 111.
 6. Lidar data at 85 km compared to lidar data at 91 km (raw data — i.e., no tidal adjustment):
Means = 180.0 ± 1.6 , 184.2 ± 1.6 . $\rho = 0.603$. Assuming $g_0 = 1$ gives $\sigma_{85} = 10$, $\sigma_{91} = 9$. Number of points = 86. If it is assumed that $\sigma_{\text{day}} = \sigma_{\text{night}}$, then $g_0 = 0.92$, $\sigma_{\text{day}} = \sigma_{\text{night}} = 9.2$.
 7. Lidar data at 85 km compared to lidar data at 88 km (raw data — i.e., no tidal adjustment):
Means = 179.6 ± 1.5 , 179.4 ± 1.5 . $\rho = 0.854$. Assuming $g_0 = 1$ gives $\sigma_{85} = 5.6$, $\sigma_{88} = 5.3$. Number of points = 98. If it is assumed that $\sigma_{\text{day}} = \sigma_{\text{night}}$, then $g_0 = 0.99$, $\sigma_{\text{day}} = \sigma_{\text{night}} = 5.5$.

The correlation coefficients shown in Table 1, and also above, are in the main significant. Confidence limits may be readily determined as follows. The function $\frac{1}{2} \ln[(1 + \rho)/(1 - \rho)]$ is normally distributed with population variance equal to $1/(n - 3)$, where n is the number of points in the sample. In our case almost all samples have close to 100 points, so if that is taken to be a typical value, then confidence limits $\rho_{1,2}$ at the 95% levels for a measured correlation coefficient ρ can be determined from the expression

$$\frac{1}{2} \ln \left[\frac{(1 + \rho_{1,2})}{(1 - \rho_{1,2})} \right] - \frac{1}{2} \ln \left[\frac{(1 + \rho)}{(1 - \rho)} \right] \approx \pm \frac{1.96}{9.8} \quad (13)$$

For example, if $\rho = 0.8$, solving gives $\rho_{1,2} = 0.72$ and 0.86 as the confidence limits. For $\rho = 0.7$, $\rho_{1,2} = 0.59$ and 0.79 , while for $\rho = 0.6$, $\rho_{1,2} = 0.46$ and 0.71 . For $\rho = 0.5$, $\rho_{1,2} = 0.34$ and 0.63 . Hence, all of our correlations are significantly nonzero.

Figure 3a shows the scatter plot of the OH temperatures and the 85 km lidar (without tidal correction) temperatures. Again the average of the data points is to the right of the equal temperature line indicating that on average the OH temperatures are warmer than the 85 km lidar temperatures.

Figure 4 is a scatter plot of the 88 km meteor temperatures and the tidally compensated 88 km lidar temperatures. The correlation of the data points is less than in the two previous figures and is reflected in the lower correlation coefficient. Again the distribution is centred to the right of the equal temperature line indicating that on average the radar temperatures are higher than the lidar temperatures.

Figure 5 is the same as Fig. 4 except that it is for 91 km temperature measurements. The envelope of the data points is spread significantly wider in the direction perpendicular to the equal temperature line for this altitude; this is reflected in a lower correlation coefficient. It is to be expected that, on average, large amplitude shorter period fluctuations, due to gravity waves, will play a more significant role at this altitude than at 88 km leading to larger variations in the measurements from the two techniques due the differences in the measurement periods. Choices in the seed temperature used for the lidar method will also be more important at the upper heights, slightly increasing lidar temperature uncertainty at 91 km (see Table 2).

Fig. 3. (a) Lidar temperatures at 95 km compared with OH temperatures for coincident nights. The means were 183.3 and 190.8, respectively. The Lidar data have not been corrected for tides since both the lidar and OH data were taken at night, but at 85 km the tide usually increases the daily average by about 4 K relative to night-time only. (b) Error determination curve. If it is accepted that both techniques measure the same temperature, then the intrinsic error in the OH method is 3.2 K and in the lidar measurements is 10.3 K.

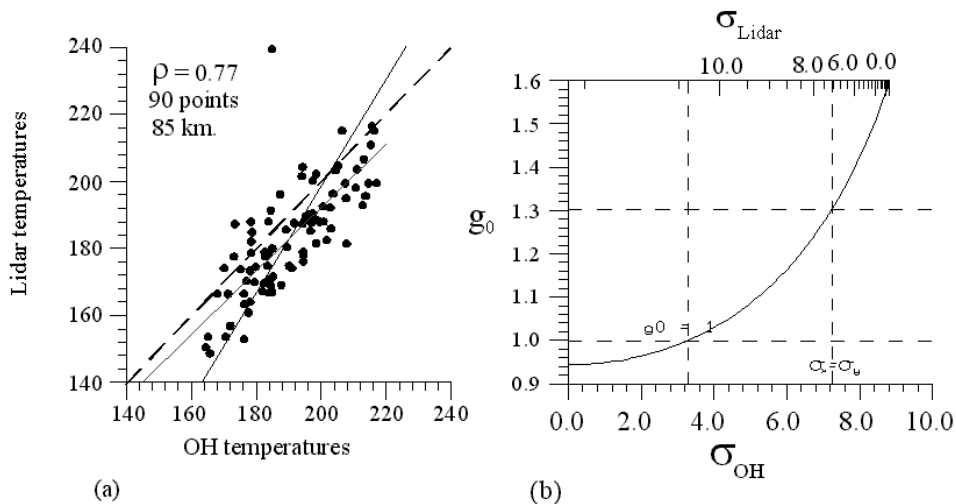
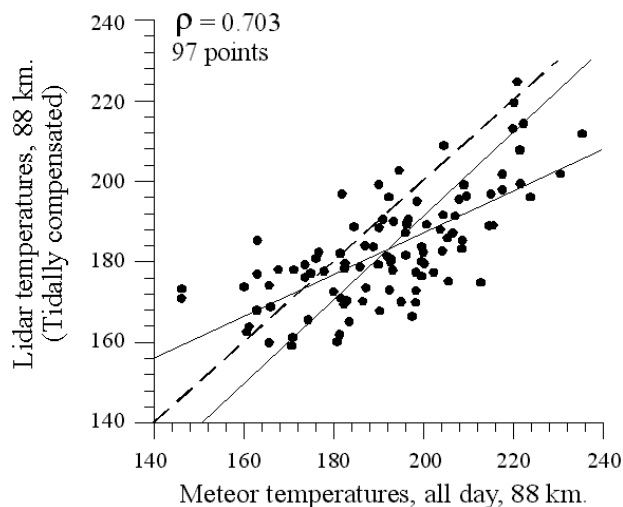


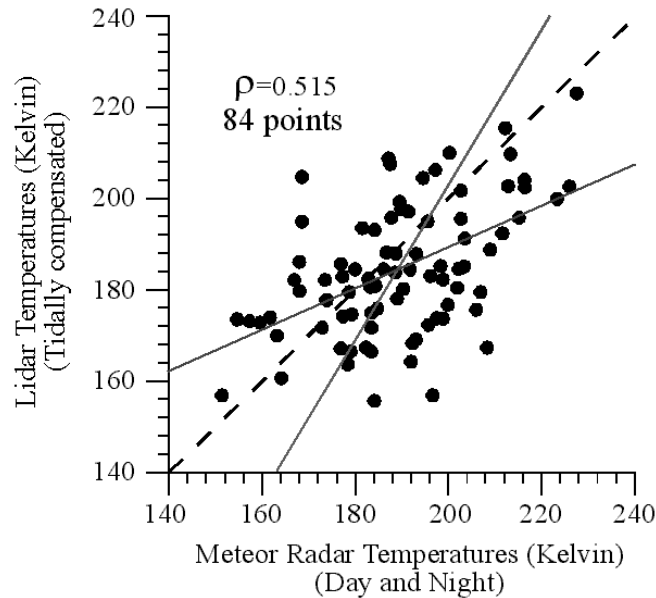
Fig. 4. Scatter plot of lidar temperatures at 88 km altitude versus meteor temperatures at 88 km. The meteor temperatures were averaged over both day and night, and the lidar data have been compensated for tidal variations. The error-determination curve is not shown to save space.



The major results of this intercomparison between the three temperature measurements methods are shown Table 1. The first line of the table compares the meteor temperatures calculated using the TG method with the lidar and OH temperatures. For the meteor–lidar comparison, the peak correlation coefficient of 0.705 occurs for the lidar range bin centered at 88 km, as might be expected since the peak of the measured meteor distribution is located within this range bin.

Table 1 shows the result of the intercomparison of the meteor radar and lidar data at each of the three altitudes and for night-only and 24 h temperatures. “Night-only data” refer to cases where the

Fig. 5. Scatter plot of lidar temperatures at 91 km altitude versus meteor temperatures at 91 km. The meteor temperatures were averaged over both day and night, and the lidar data have been compensated for tidal variations. The error-determination curve is not shown to save space.



meteor data were restricted to night-time measurements only — of course the lidar data are all night-time only. The correlation coefficients are not significantly different for the 24 h versus night only data sets. The average temperatures for the two data sets compare differently at different altitudes. At 85 km the average of the night time only measurements for the lidar is 0.7 K warmer than the corresponding meteor radar average. Given the errors shown, this difference is not significant at to the 95% level, as determined using a Student t-test. At 88 km the lidar average is 11 K colder for the night only average and 9.3 K colder for the 24 h average, while at 91 km the lidar average is about 5 K colder for both the night only and 24 h averages. These differences are statistically significant at the 95% level and indicate systematic differences in the two techniques.

The average meteor radar temperature, over the entire meteor detection region, is only 1.6 K cooler than the average OH temperature. When considering the temperatures in each of the meteor radar height bins the differences from the OH temperatures range from 3.4 K warmer (88 km, 24 h) to 4.1 K colder (85 km, night only). The correlation coefficients between the OH and 24 h meteor radar measurements are 0.706, 0.720, and 0.659 for meteor heights of 85, 88, and 91 km, respectively. This indicates that the peak of the OH layer, the altitude which influences the OH temperature most significantly, is likely just below 88 km. This is in good agreement with previous estimates [3] of 87 km as the mean altitude of the OH layer.

The average lidar temperature is lower than the OH temperature by 7.5, 5.8, and 2.3 K for the 85, 88, and 91 km lidar range bins, respectively. This is somewhat surprising as these two methods could be expected, because of their similar horizontal and spatial resolution, to be similar, particularly when the mean altitude of the OH layer is known to be slightly below the centre of the central lidar range bin. The difference probably emphasizes the difficulties in interpretation of passive optical measurements of temperature due to uncertainties in the height profile of the emission.

It is also noteworthy that the correlation between the mean meteor temperatures by the TG method (no height information) and the lidar temperatures at the different heights of 85, 88, and 91 km, and the correlations between height-dependent (TGE method) meteor and lidar temperatures on a height-by-height basis, are comparable.

If the new meteor method is truly useful, an improvement in correlation might be expected with the height-by-height comparison. The fact that this does not occur might suggest that the new meteor method may not be useful, even though in principle it should be effective. However, there is considerable geophysical variability, and many differences associated with each method, which may mask such an effect. It is not at all surprising that the yearly variation at 85 and 88 and 91 km should be very similar, and so the major contributor to the correlation between the different data is the annual variability. Small differences between temporal variations in temperatures at nearby heights may be lost in the noise. At this stage, then, we can only say that the new meteor method does not degrade the meteor temperature quality, but further studies are needed, using larger data sets, and possibly by breaking the data into different seasons, to ascertain whether the height-dependent meteor temperatures really do represent a useful improvement over the mean meteor temperatures.

4. Conclusions

We have compared 104 dates of meteor radar with lidar data and 116 dates of meteor radar with hydroxyl rotational data. Comparisons of this type are hindered as it is difficult to separate instrumental differences from geophysical differences. Considering that each instrument is measuring different spatial averages, the correlation coefficients of the meteor radar and the lidar at the lower heights (85, 88 km), 0.60 to 0.70, can be considered satisfactory. The correlation coefficients at the upper height (91 km), 0.47 to 0.51, seem to show less correlation between the two systems. This may be due to enhanced gravity-wave activity at the upper heights. The correlation coefficients of the meteor radar and the hydroxyl rotational method are between 0.62 and 0.73, and this is satisfactory. We have shown that the meteor radar is making consistent measurements for the 85 and 88 km heights. The usefulness of a new height-dependent meteor temperature method has been studied, but it is hard to determine how accurate the new method is because of the dominating effect of geophysical noise in height-by-height comparisons. Further studies of this new method are warranted.

This study provides a guide to the accuracy of meteor radar, hydroxyl rotational, and lidar temperatures in the mesopause region. Each instrument has separate advantages and disadvantages. Radar measurements cover both day and night, and meteor radars run without the need for user intervention. The lidar provides high temporal-spatial resolution, and the hydroxyl rotational method provides measurements every 30 s. On average, all methods gave similar measurements for 85 and 88 km heights, with their mean values showing high correlation at these levels. However, there is only weak correlation between the meteor radar and lidar temperatures at 91 km, possibly due to increased gravity wave activity at the upper heights, which introduces greater variability between the two methods.

Acknowledgements

This work is partly supported by the Natural Sciences and Engineering Research Council of Canada, through grants to W. Hocking, R. Sica, and R. Lowe. Funding for the hydroxyl measurements was provided by the Centre for Research in Earth and Space Technology, An Ontario Centre-of-Excellence.

References

1. W.K. Hocking, W. Singer, J. Bremer, N.J. Mitchell, P. Batista, B. Clemesha, and M. Donner. *J. Atmos. Solar-Terr. Phys.* **66**, 585 (2004).
2. C.M. Hall, T. Aso, M. Tsutsumi, J. Höffner, and F. Sigernes. *Radio Sci.* **39**, RS6001 (2004).
3. C.Y. She and R.P. Lowe. *J. Atmos. Solar-Terr. Phys.* **60**, 1573 (1998).
4. W.K. Hocking and T. Thayaparan. *Radio Sci.* **32**, 833 (1997).
5. W.K. Hocking, B. Fuller, and B. Vandeppeer. *J. Atmos. Solar-Terr. Phys.* **63**, 155 (2001).
6. J. Jones, A.R. Webster, and W.K. Hocking. *Radio Sci.* **33**, 55 (1998).
7. R.J. Sica, S. Sargoytchev, P.S. Argall, E.F. Borra, L. Girard, C.T. Sparrow, and S. Flatt. *Appl. Opt.* **34**, 6925 (1995).

8. R.P. Lowe, K.L. Gilbert, and D.N. Turnbull. *Planet Space Sci.* **39**, 1263 (1991).
9. D.N. Turnbull and R.P. Lowe. *Can. J. Phys.* **61**, 244 (1983).
10. P.B. Chilson, P. Czechowsky, and G. Schmidt. *Geophys. Res. Lett.* **23**, 2745 (1996).
11. W.K. Hocking, T. Thayaparan, and J. Jones. *Geophys. Res. Lett.* **24**, 2977 (1997).
12. E.L. Fleming, S. Chandra, M.R. Schoerberl, and J.J. Bennett. NASA Technical Memorandum 100697. 1988.
13. W.K. Hocking. *Geophys. Res. Lett.* **26**, 3297 (1999).
14. W.K. Hocking and A. Hocking. *Ann. Geophys.* **20**, 1447 (2002).
15. GSWM-02. <http://sisko.colorado.edu/TIMED/GSWM.html>
16. W.K. Hocking, T. Thayaparan, and S.J. Franke. *Adv. Space Res.* **27**, 6, 1089 (2001).
17. A.Z. Liu, K.W. Hocking, S.J. Franke, and T. Thayaparan. *Atmos. Solar-Terrestrial Phys.* **64**, 31 (2001).